

Finite element formulations for free field one-dimensional shear wave propagation

Sun-Hoon Kim^{*1} and Kwang-Jin Kim^{2b}

¹Department of Civil and Environmental Engineering, U1 University, Yeoungdong-kun, Chungbuk 29131, Republic of Korea

²Comtec Research, Seocho-ku, Seoul 06650, Republic of Korea

(Received August 28, 2023, Revised September 25, 2023, Accepted January 10, 2024)

Abstract. Dynamic equilibrium equations for finite element analysis were derived for the free field one-dimensional shear wave propagation through the horizontally layered soil deposits with the elastic half-space. We expressed Rayleigh's viscous damping consisting of mass and stiffness proportional terms. We considered two cases where damping matrices are defined in the total and relative displacement fields. Two forms of equilibrium equations are presented; one in terms of total motions and the other in terms of relative motions. To evaluate the performance of new equilibrium equations, we conducted two sets of site response analyses and directly compared them with the exact closed-form frequency domain solution. Results show that the base shear force as earthquake load represents the simpler form of equilibrium equation to be used for the finite element method. Conventional finite element procedure using base acceleration as earthquake load predicts exact solution reasonably well even in soil deposits with unrealistically high damping.

Keywords: base acceleration; base shear force; dynamic equilibrium equation; elastic half-space; free field analysis; shear wave propagation

1. Introduction

Recent research in wave motion is mainly focused on transient phenomena occurring in wave loadings as well as earthquakes. In particular, free field one-dimensional shear wave propagation to earthquakes is a subject of intense concern to many civil engineers (Liu *et al.* 2017, Watanabe *et al.* 2017).

This study mainly focused on the formulations of dynamic equilibrium equations that apply to finite element procedures under the following simplified ideal conditions:

- Soil deposit consists of homogeneous and isotropic viscoelastic infinite horizontal layers.
- Bedrock is overlying an elastic half-space absorbing downward reflected shear waves.
- Earthquake load is applied at the bedrock surface as an incident shear wave propagating vertically.

For such a one-dimensional wave propagation problem, there are currently two different formulations used by finite element analysis (Tran *et al.* 2021, Volpini *et al.* 2021).

The first one is the conventional method where earthquake outcrop acceleration is directly applied at the bottom of the soil deposit as an external load and the bottom boundary may be assumed to be rigid or energy absorbing to represent elastic half-space. The dynamic equilibrium equation is expressed in terms of relative

motions concerning base outcrop motions. This method, here named **BAC** (Base Acceleration Conventional), has been used for many decades in the finite element analysis community.

The other one is a relatively new method where the base shear force, associated with the base outcrop velocity, is applied at the bottom of the soil deposit as an external load along with energy absorbing viscous damper representing the elastic half-space. The dynamic equilibrium equation in this unconstrained system is expressed in terms of total particle motions. This method, here named **BST** (Base Shear Total), was first proposed by Tsai (1969) and then by Joyner and Chen (1975). The equilibrium equation is derived based on the principles of shear waves propagating through the soil deposit from the elastic bedrock.

Now, questions arise over these two different methods. The first question is "Can these two methods be correlated to each other?". The second question is "Can other forms of equilibrium equations be derived based on the second method **BST**?". To answer such questions, we reformulated the **BST** method under two separate conditions; the first case is where the damping matrix is defined in the total displacement fields and the other case is where the damping matrix is defined in the relative displacement fields concerning interface displacements at bedrock.

The main outcomes of this study include the following. There are four different exact formulations derived from the definition of damping matrix and the selection of motion variables. Such a new formulation (**BAT**) identifies what is missing in the conventional formulation (**BAC**) to represent earthquake load more accurately. The other outcome shows why the **BST** model is a simpler and computationally favorable formulation compared to the other models.

*Corresponding author, Professor

E-mail: kimsh@yd.ac.kr

^aPh.D. Principal Engineer

E-mail: info@comtecresearch.co.kr

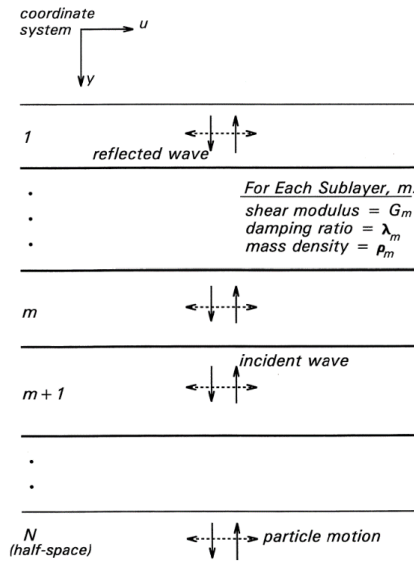


Fig. 1 One-dimensional system over a uniform half-space

To evaluate the performance of new equilibrium equations, we conducted two sets of site response analyses for the 1989 Diamond Heights earthquake (Germoso *et al.* 2020) and the 1995 Kobe earthquake (Xu *et al.* 2023) and directly compared them with SHAKE91 (Idriss and Sun 1992, Astroza *et al.* 2017) which represents exact, under the above-mentioned simplified conditions, closed-form solution performed in the frequency domain.

2. Frequency domain analysis

Understanding basic principles in frequency domain analysis is probably the most valuable benefit in deriving the formulations for finite element analysis which is performed in the time domain.

Frequency domain analysis has been used for the solution of site responses subjected to vertically propagating shear waves as schematically shown in Fig. 1. For such analysis, SHAKE (Schnabel *et al.* 1972, Ameri *et al.* 2023) has been the most popular computer program because of its simplicity and practicality in using the program. Since SHAKE, more recent versions have been written to improve the user interface and to show graphical outputs such as SHAKE91 and SHAKE2000 (Ordonez 2012, Chatterjee *et al.* 2015, Ghaemmaghami *et al.* 2017).

The main characteristics of the wave motions in the horizontally layered system may be described such as in the following statements. In each layer, the horizontal particle motion consists of the upward incident wave and the downward reflected wave. On the interface between the adjacent layers, displacements and stresses are continuous. On the top surface, the amplitude of an incident wave is the same as that of the reflected wave since the shear stresses should be zero on such a free ground surface. Thus, the amplitude on the top surface is equal to twice the magnitude of the incident wave. On the bottom surface, the downward reflected wave is absorbed into the elastic half-space so that the upward incident wave will not be interrupted by the

overlying soil deposit. It should be noted that such an upward incident wave is half the magnitude of “outcrop bedrock motion” for the same reason as explained for the top-ground surface.

The main algorithms of the frequency domain analysis may be described in the following way. For each harmonic motion, set up transfer functions for the incident and reflected waves in each layer, refer to SHAKE for the detailed derivation. These transfer functions represent the ratio of amplitudes in a layer to those at the top surface. The input object accelerations in the time domain are converted to Fourier series form in the frequency domain using the Fast Fourier Transform (FFT) method. Amplitudes at any location in the layer can be found by using Fourier series and transfer functions in the frequency domain and then responses in the time domain can be determined by inverting FFT.

3. Shear stress on the surface of elastic half-space

As illustrated in Fig. 1, the horizontal particle velocity (\dot{u}) on the bottom surface consists of two components; incident velocity (\dot{u}_I) and reflected velocity (\dot{u}_R) which are associated with upward propagating incident and downward propagating reflected waves, respectively.

$$\dot{u} = \dot{u}_I + \dot{u}_R \quad (1)$$

Consequently, shear stress (τ) on the bottom surface can be thought of as having two components; (τ_I) and (τ_R) which are associated with incident and reflected waves, respectively.

$$\tau = \tau_I + \tau_R \quad (2)$$

Considering radiation boundary conditions on the surface of half-space, we can obtain the following two equations related to the upward incident and downward reflected waves.

$$\tau_I = \rho_r \cdot c_{sr} \cdot \dot{u}_I \quad (3)$$

$$\tau_R = -\rho_r \cdot c_{sr} \cdot \dot{u}_R \quad (4)$$

where ρ_r is rock mass density and c_{sr} is rock shear wave velocity.

Noting that the incident wave is half the magnitude of “outcrop bedrock motion” as explained in the previous section, the incident particle velocity (\dot{u}_I) can be related to the input outcrop earthquake velocity (\dot{u}_g) as

$$\dot{u}_I = \frac{1}{2} \dot{u}_g \quad (5)$$

Substituting Eq. (5) into Eq. (3)

$$\tau_I = \rho_r \cdot c_{sr} \cdot \left(\frac{1}{2} \dot{u}_g\right) \quad (6)$$

From Eqs. (1) and (5), reflected particle velocity (\dot{u}_R) can be expressed in terms of total particle velocity and earthquake outcrop velocity on the surface of elastic half-space.

$$\dot{u}_R = \dot{u} - \frac{1}{2} \dot{u}_g \quad (7)$$

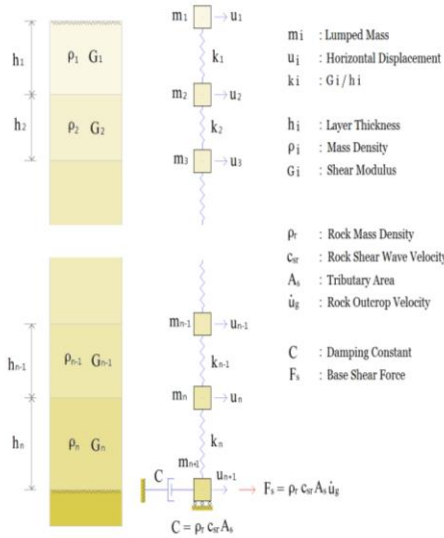


Fig. 2 One-dimensional shear wave propagation including elastic half-space

Substituting Eq. (7) into Eq. (4)

$$\tau_R = -\rho_r \cdot c_{sr} \cdot \left(\dot{u} - \frac{1}{2} \dot{u}_g \right) \quad (8)$$

Now, substituting Eqs. (6) and (8) into Eq. (2), the shear stress on the surface of elastic half-space can be expressed in terms of total particle velocity and earthquake outcrop velocity.

$$\tau = \rho_r \cdot c_{sr} \cdot \dot{u}_g - \rho_r \cdot c_{sr} \cdot \dot{u} \quad (9)$$

In Eq. (9), the first term represents the shear stress driven by the input earthquake. The second term represents the shear stress associated with the transmitted energy absorbed into the elastic half-space (Tsai 1969, Desai and Christian 1977).

Such shear stress (τ) can be converted to shear force (F) considering tributary area (A_s)

$$F = F_s - C \cdot \dot{u} \quad (10)$$

Where the base shear force (F_s) and damping constant (C) are given by

$$F_s = C \cdot \dot{u}_g \quad (11)$$

$$C = \rho_r \cdot c_{sr} \cdot A_s \quad (12)$$

Eq. (10) will be incorporated into the finite element formulations in the next sections.

4. When the damping matrix is defined in total displacement

4.1 Exact formulation (BAT model)

In the previous section, shear force on the surface of elastic half-space was interpreted as the contribution of both base shear force (F_s) driven by input earthquake load and transmitted force ($C \cdot \dot{u}_{n+1}$) through viscous damper as

schematically illustrated with the analogy of shear-beam in Fig. 2.

In this section, we assume that damping and stiffness matrices are defined in total displacement. Then the dynamic equilibrium equation for the one-dimensional shear wave propagation through soil deposit with elastic half-space is given in the following matrix form.

Named **BST** (Base Shear Total)

$$\mathbf{M}\ddot{\mathbf{u}} + \mathbf{D}\dot{\mathbf{u}} + \mathbf{K}\mathbf{u} + \mathbf{J} \cdot \mathbf{C} \cdot \dot{u}_{n+1} = \mathbf{J} \cdot F_s \quad (13)$$

where \mathbf{M} , \mathbf{D} and \mathbf{K} represent mass, damping, and stiffness matrices, respectively.

And \mathbf{u} , $\dot{\mathbf{u}}$ and $\ddot{\mathbf{u}}$ represent total displacement, velocity, and acceleration vectors, respectively.

(\dot{u}_{n+1}) is the interface total velocity and the vector with the unit at only the last row \mathbf{J} is given by

$$\mathbf{J}^T = \langle 0, 0, \dots, 0, 0, 1 \rangle \quad (14)$$

Defining the total displacement \mathbf{u} as the sum of relative displacement \mathbf{u}_r and outcrop base displacement u_g and rewriting Eq. (13) in terms of the relative motions,

$$\mathbf{M}(\ddot{\mathbf{u}}_r + \mathbf{I} \cdot \ddot{u}_g) + \mathbf{D}(\dot{\mathbf{u}}_r + \mathbf{I} \cdot \dot{u}_g) + \mathbf{K}(\mathbf{u}_r + \mathbf{I} \cdot u_g) + \mathbf{J} \cdot \mathbf{C} \cdot (\dot{u}_{r,n+1} + \dot{u}_g) = \mathbf{J} \cdot F_s \quad (15)$$

\mathbf{u}_r , $\dot{\mathbf{u}}_r$ and $\ddot{\mathbf{u}}_r$ represent relative displacement, velocity, and acceleration vectors, respectively. u_g , \dot{u}_g and \ddot{u}_g also represent rock outcrop displacement, velocity, and acceleration, respectively.

(\dot{u}_{rn+1}) is the interface relative velocity and the vector with unit at all rows \mathbf{I} is given by

$$\mathbf{I}^T = \langle 1, 1, \dots, 1, 1, 1 \rangle \quad (16)$$

The lumped mass system in Fig. 2 is statically unconstrained so the following term in Eq. (15) will have vanished since it represents the rigid body movement.

$$\mathbf{K} \cdot \mathbf{I} = \mathbf{0} \quad (17)$$

It is a quite common practice to express the viscous damping by Rayleigh et al. (1945) which consists of mass and stiffness proportional terms (a and b) in the element level.

$$\mathbf{D} = a \cdot \mathbf{M} + b \cdot \mathbf{K} \quad (18)$$

Now, substituting Eqs. (17) and (18) into Eq. (15) and rearranging,

$$\begin{aligned} & \mathbf{M}\ddot{\mathbf{u}}_r + \mathbf{D}\dot{\mathbf{u}}_r + \mathbf{K}\mathbf{u}_r + \mathbf{J} \cdot \mathbf{C} \cdot \dot{u}_{rn+1} \\ & = -\mathbf{M} \cdot \mathbf{I} \cdot \ddot{u}_g - a \cdot \mathbf{M} \cdot \mathbf{I} \cdot \dot{u}_g + \mathbf{J} \cdot (F_s - C \cdot \dot{u}_g) \end{aligned} \quad (19)$$

The last term in Eq. (19) will have vanished since $F_s = C \cdot \dot{u}_g$. Thus the final equilibrium equation in terms of relative motions can be expressed in the following matrix form: Named **BAT** (Base Acceleration Total)

$$\begin{aligned} & \mathbf{M}\ddot{\mathbf{u}}_r + \mathbf{D}\dot{\mathbf{u}}_r + \mathbf{K}\mathbf{u}_r + \mathbf{J} \cdot \mathbf{C} \cdot \dot{u}_{rn+1} \\ & = -\mathbf{M} \cdot \mathbf{I} \cdot \ddot{u}_g - a \cdot \mathbf{M} \cdot \mathbf{I} \cdot \dot{u}_g \end{aligned} \quad (20)$$

It should be noted that **BAT** in Eq. (20) in relative motions is simply the alternate form of **BST** in Eq. (13) in total motions. Both **BST** and **BAT** models will give the same analysis results as demonstrated in the example

problems included in this study.

4.2 Conventional formulation (**BAC** model)

Conventional finite element formulations (Desai and Christian 1977, Dikmen and Ghaboussi 1984, Hudson *et al.* 1994) for the seismic response of ground motion are expressed in the following matrix form simply by adding damping forces to the left side of dynamic equilibrium equation without considering the consistent definition of damping matrix in the total displacement fields.

$$\mathbf{M}\ddot{\mathbf{u}}_r + \mathbf{D}\dot{\mathbf{u}}_r + \mathbf{K}\mathbf{u}_r + \mathbf{J} \cdot \mathbf{C} \cdot \dot{\mathbf{u}}_{rn+1} = -\mathbf{M} \cdot \mathbf{I} \cdot \ddot{\mathbf{u}}_g \quad (21)$$

When there is no mass proportional damping term ($a=0$), the **BAT** model in Eq. (20) represents the conventional finite element procedure where only base outcrop acceleration is applied for earthquake load: Named **BAC** (Base Acceleration Conventional)

However, when there is mass proportional damping ($a \neq 0$), the **BAT** model in Eq. (20) includes the outcrop velocity term in addition to the acceleration term to represent earthquake load more accurately. The effect of such additional earthquake velocity term may be insignificant for most practical problems based on our studies presented in the following example problems. It is worth noting that the **BAC** model in Eq. (21) has been used for many decades in the finite element analysis communities for structural and geotechnical engineering problems.

5. When the damping matrix is defined in relative displacement

In this section, we assume that damping and stiffness matrices are defined in relative displacement. Then the dynamic equilibrium equation for the one-dimensional shear wave propagation through soil deposit with elastic half-space is given in the following matrix form.

$$\mathbf{M}\ddot{\mathbf{u}} + \mathbf{D}(\dot{\mathbf{u}} - \mathbf{I} \cdot \dot{\mathbf{u}}_{n+1}) + \mathbf{K}(\mathbf{u} - \mathbf{I} \cdot \mathbf{u}_{n+1}) + \mathbf{J} \cdot \mathbf{C} \cdot \dot{\mathbf{u}}_{n+1} = \mathbf{J} \cdot \mathbf{F}_s \quad (22)$$

Substituting Eq. (18) into Eq. (22), we obtain the following equation.

$$\mathbf{M}\ddot{\mathbf{u}} + \mathbf{D}\dot{\mathbf{u}} - (\mathbf{a} \cdot \mathbf{M} + \mathbf{b} \cdot \mathbf{K}) \cdot \mathbf{I} \cdot \dot{\mathbf{u}}_{n+1} + \mathbf{K}(\mathbf{u} - \mathbf{I} \cdot \mathbf{u}_{n+1}) + \mathbf{J} \cdot \mathbf{C} \cdot \dot{\mathbf{u}}_{n+1} = \mathbf{J} \cdot \mathbf{F}_s \quad (23)$$

Substituting Eq. (17) into Eq. (23), we obtain the equation in terms of total displacement.

Named **BSR** (Base Shear Relative)

$$\mathbf{M}\ddot{\mathbf{u}} + \mathbf{D}\dot{\mathbf{u}} + \mathbf{K}\mathbf{u} + (\mathbf{C} \cdot \mathbf{J} - \mathbf{a} \cdot \mathbf{M} \cdot \mathbf{I}) \cdot \dot{\mathbf{u}}_{n+1} = \mathbf{J} \cdot \mathbf{F}_s \quad (24)$$

Note that both **BST** in Eq. (13) and **BSR** in Eq. (24) are expressed in terms of total displacements. However, when the damping matrix is defined in the relative displacement, an additional term that is related to Rayleigh mass proportional constant (a) is enclosed in the equilibrium equation.

Now, we want to define the total displacement \mathbf{u} in Eq. (24) as the sum of relative displacement \mathbf{u}_r and outcrop

base displacement \mathbf{u}_g as we have done for Eq. (15).

$$\mathbf{M}(\ddot{\mathbf{u}}_r + \mathbf{I} \cdot \ddot{\mathbf{u}}_g) + \mathbf{D}(\dot{\mathbf{u}}_r + \mathbf{I} \cdot \dot{\mathbf{u}}_g) + \mathbf{K}(\mathbf{u}_r + \mathbf{I} \cdot \mathbf{u}_g) + (\mathbf{C} \cdot \mathbf{J} - \mathbf{a} \cdot \mathbf{M} \cdot \mathbf{I}) \cdot (\dot{\mathbf{u}}_{rn+1} + \dot{\mathbf{u}}_g) = \mathbf{J} \cdot \mathbf{F}_s \quad (25)$$

Substituting Eqs. (17) and (18) into Eq. (25), we obtain the following equation.

$$\mathbf{M}(\ddot{\mathbf{u}}_r + \mathbf{I} \cdot \ddot{\mathbf{u}}_g) + \mathbf{D}\dot{\mathbf{u}}_r + \mathbf{a} \cdot \mathbf{M} \cdot \mathbf{I} \cdot \dot{\mathbf{u}}_g + \mathbf{K}\mathbf{u}_r + (\mathbf{C} \cdot \mathbf{J} - \mathbf{a} \cdot \mathbf{M} \cdot \mathbf{I}) \cdot (\dot{\mathbf{u}}_{rn+1} + \dot{\mathbf{u}}_g) = \mathbf{J} \cdot \mathbf{F}_s \quad (26)$$

Eq. (26) can be rearranged in the following form.

$$\mathbf{M}\ddot{\mathbf{u}}_r + \mathbf{D}\dot{\mathbf{u}}_r + \mathbf{K}\mathbf{u}_r + (\mathbf{C} \cdot \mathbf{J} - \mathbf{a} \cdot \mathbf{M} \cdot \mathbf{I}) \cdot \dot{\mathbf{u}}_{rn+1} = -\mathbf{M} \cdot \mathbf{I} \cdot \ddot{\mathbf{u}}_g + \mathbf{J} \cdot (\mathbf{F}_s - \mathbf{C} \cdot \dot{\mathbf{u}}_g) \quad (27)$$

The last term in Eq. (27) will have vanished since $\mathbf{F}_s = \mathbf{C} \cdot \dot{\mathbf{u}}_g$. Thus the final equilibrium equation in terms of relative motions can be expressed in the following matrix form.

Named **BAR** (Base Acceleration Relative)

$$\mathbf{M}\ddot{\mathbf{u}}_r + \mathbf{D}\dot{\mathbf{u}}_r + \mathbf{K}\mathbf{u}_r + (\mathbf{C} \cdot \mathbf{J} - \mathbf{a} \cdot \mathbf{M} \cdot \mathbf{I}) \cdot \dot{\mathbf{u}}_{rn+1} = -\mathbf{M} \cdot \mathbf{I} \cdot \ddot{\mathbf{u}}_g \quad (28)$$

Comparing **BAR** in Eq. (28) to **BSR** in Eq. (24), both models show similar forms on the left side of the equal sign while on the right side of the equal sign, one is driven by base shear force in **BSR** and the other by base acceleration in **BAR**. Both models contain a term with the product of $(\mathbf{a} \cdot \mathbf{M} \cdot \mathbf{I})$ and the interface velocity $(\dot{\mathbf{u}}_{n+1}, \dot{\mathbf{u}}_{rn+1})$. The inclusion of such a term can lead to a non-symmetric full matrix for the solution. To take advantage of the banded symmetric matrix form, we can move this term to the right-hand side of the equal sign and then perform iterations or use smaller time increments.

6. Step-by-step solution

6.1 Linear elastic formulation

To complete finite element formulation for one-dimensional shear wave propagation, we include a direct integration procedure for the case when the damping matrix is defined in the total displacement field.

Eqs. (13) and (20) may be expressed in the following matrix form at time step i .

$$\mathbf{M}\ddot{\mathbf{u}}_i + \mathbf{D}\dot{\mathbf{u}}_i + \mathbf{K}\mathbf{u}_i = \mathbf{R}_i \quad (29)$$

$$\mathbf{R}_i = -\mathbf{M} \cdot \mathbf{I} \cdot (\ddot{\mathbf{u}}_{gni} + \mathbf{a} \cdot \dot{\mathbf{u}}_{gni})$$

when \mathbf{u}_i represents relative displacement

$$\mathbf{R}_i = \mathbf{J} \cdot \rho_r \cdot c_{sr} \cdot A_s \cdot \dot{\mathbf{u}}_{gni}$$

when \mathbf{u}_i represent total displacement

It should be noted that the damping matrix in Eq. (29) incorporated implicitly shear forces related to radiation boundary conditions representing the elastic half-space.

For the direct time integration of Eq. (29), Newmark constant average acceleration method (Newmark 1959), which is unconditionally stable, may be used. For constant time increment Δt ,

$$\ddot{\mathbf{u}}_i = \ddot{\mathbf{u}}_{i-1} + (\ddot{\mathbf{u}}_{i-1} + \ddot{\mathbf{u}}_i) \cdot (\Delta t/2) \quad (30)$$

$$\mathbf{u}_i = \mathbf{u}_{i-1} + \dot{\mathbf{u}}_{i-1} \cdot \Delta t + (\ddot{\mathbf{u}}_{i-1} + \ddot{\mathbf{u}}_i) \cdot (\Delta t^2 / 4) \quad (31)$$

From Eqs. (30) and (31), we can obtain the following equations.

$$\ddot{\mathbf{u}}_i = (4/\Delta t^2) \cdot \mathbf{u}_i - \mathbf{A}_{i-1} \quad (32)$$

$$\dot{\mathbf{u}}_i = (2/\Delta t) \cdot \mathbf{u}_i - \mathbf{B}_{i-1} \quad (33)$$

where

$$\mathbf{A}_{i-1} = 4 \cdot (\mathbf{u}_{i-1}/\Delta t^2 + \dot{\mathbf{u}}_{i-1}/\Delta t + \ddot{\mathbf{u}}_{i-1}/4) \quad (34)$$

$$\mathbf{B}_{i-1} = 2 \cdot (\mathbf{u}_{i-1}/\Delta t) + \dot{\mathbf{u}}_{i-1} \quad (35)$$

Substituting Eqs. (32) and (33) into Eq. (29), we obtain the following equation.

$$\bar{\mathbf{K}} \cdot \mathbf{u}_i = \bar{\mathbf{R}}_i \quad (36)$$

$$\bar{\mathbf{K}} = (4/\Delta t^2) \cdot \mathbf{M} + (2/\Delta t) \cdot \mathbf{D} + \mathbf{K} \quad (37)$$

$$\bar{\mathbf{R}}_i = \mathbf{R}_i + \mathbf{M} \cdot \mathbf{A}_{i-1} + \mathbf{D} \cdot \mathbf{B}_{i-1} \quad (38)$$

The energy loss associated with viscous damping in Eq. (18) is proportional to the velocity, which also depends on the frequency of the motion. The energy dissipation in soils, however, is independent of frequency even at very small strain levels based on experimental test data (Lai and Rix 1988). Based on recent studies (Payan *et al.* 2016b, Senetakis and Payan 2018), small strain dampings in sand and silty sand are most influenced by confining pressure, gradation, and particle shape among others. To mitigate such a frequency dependency in Rayleigh damping, the values of (a) and (b) in Eq. (18) are expressed in terms of two target frequencies (ω_1 and ω_i) (Hudson 1994).

$$a = 2 \cdot \beta \cdot \omega_1 \cdot \omega_i / (\omega_1 + \omega_i) \quad (39)$$

$$b = 2 \cdot \beta / (\omega_1 + \omega_i) \quad (40)$$

where ω_1 represents the fundamental natural circular frequency of the system, ω_i represents the predominant circular frequency of the input earthquake motion and β represents the critical damping ratio in an element.

Five different modeling options are implemented in the general-purpose finite element computer program SMAP-3D (Comtec Research 2022) using the following abbreviations to represent each model:

- **BST**- **B**ase **S**hear where **T**otal displacement in defining damping matrix, Eq. (13)
- **BAT**- **B**ase **A**cceleration where **T**otal displacement in defining damping matrix, Eq. (20)
- **BAC**- **B**ase **A**cceleration where **C**onventional finite element procedure is used, Eq. (21)
- **BSR**- **B**ase **S**hear where **R**elative displacement in defining damping matrix, Eq. (24)
- **BAR**- **B**ase **A**cceleration where **R**elative displacement in defining damping matrix, Eq. (28)

6.2 Nonlinear elasto-plastic formulation

For the nonlinear elasto-plastic soils, Eq. (29) can be rewritten in the following form.

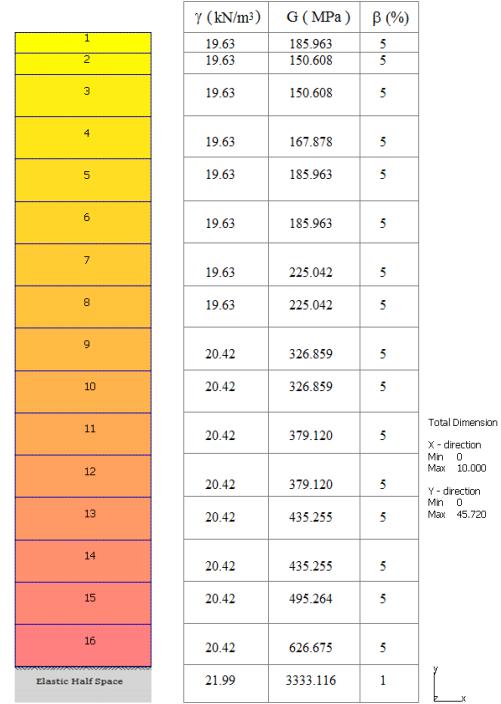


Fig. 3 Finite element meshes and material properties for Problem 1

$$\mathbf{M}\ddot{\mathbf{u}}_i + \mathbf{D}\dot{\mathbf{u}}_i + \mathbf{K}_t\Delta\mathbf{u}_i = \mathbf{R}_i - \mathbf{R}_{i-1} \quad (41)$$

where \mathbf{K}_t Tangent stiffness matrix, $\Delta\mathbf{u}_i$ Total displacement increment vector, and \mathbf{R}_{i-1} Internal resisting force vector computed from stresses at the previous step. Eq. (41) can be expressed as a set of linear equations in a similar way as Eq. (36) is derived.

7. Numerical examples

7.1 Problem 1: Site response analysis to Diamond Heights earthquake

The first example problem is the site response analysis to the Diamond Heights earthquake. The main purpose of this site response analysis is to verify that the base acceleration **BAT** model in terms of relative motions will produce the same results as the base shear **BST** model in terms of total motions. The second purpose is to assess the accuracy of the conventional finite element base acceleration **BAC** model where the equilibrium equation does not include the last term in the **BAT** model.

This example problem is the same as the sample problem in SHAKE91. A 45.72 m (150 ft) soil profile was subjected to the Diamond Heights earthquake in 1989 as an outcrop to the elastic half-space. The earthquake is scaled to a peak acceleration of 0.1g. Finite element meshes and material properties are shown in Fig. 3. The scaled earthquake time history and its spectral acceleration are shown in Figs. 4 and 5, respectively. The predominant period of the earthquake is about 0.4 seconds as shown in the response spectrum.

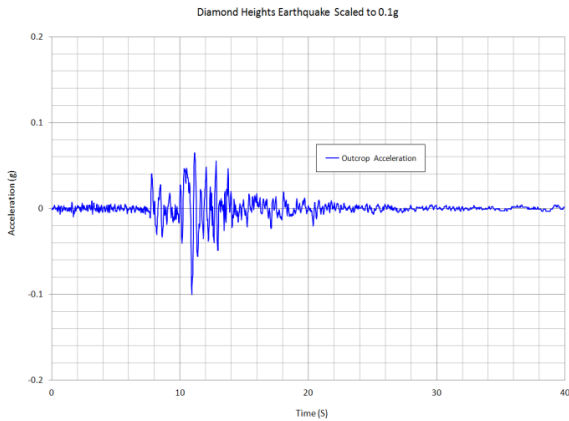


Fig. 4 Diamond Heights acceleration time history

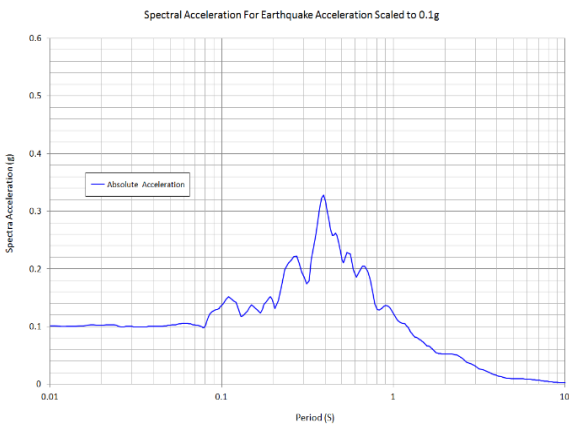


Fig. 5 Spectral acceleration for scaled Diamond Heights earthquake

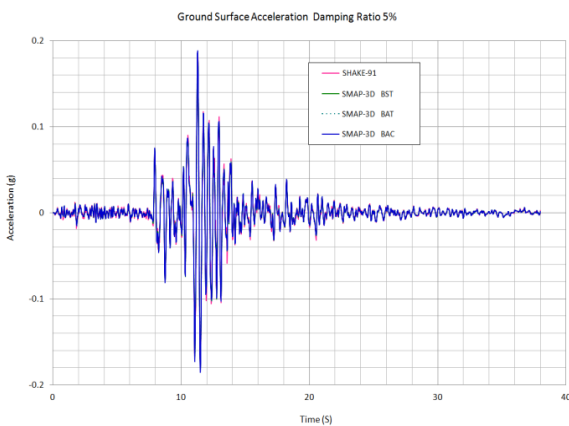


Fig. 6 Ground surface accelerations with 5% soil damping

The shear moduli in Fig. 3 represent the maximum values taken from the reference (Idriss and Sun 1992). These maximum shear moduli are often expressed as a function of void ratio, overconsolidation ratio, and effective mean principal stress (Hardin and Drnevich 1972a, b). Based on recent studies (Payan 2017, Payan *et al.* 2016a), the maximum shear modulus of sands can be more accurately computed by considering grain size distribution and particle shape in addition to the void ratio and confining pressure.

As the first set of analyses, we considered 5% soil

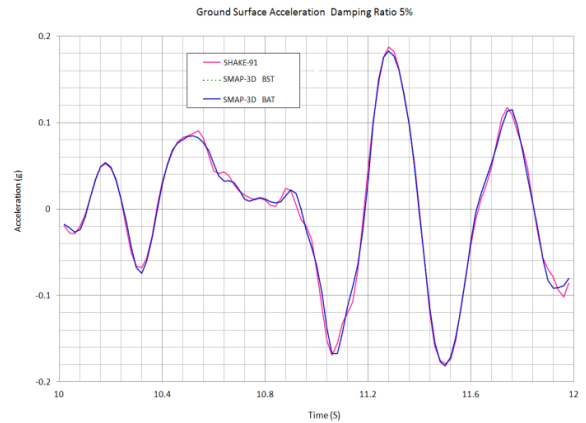


Fig. 7 Accelerations from 10 to 12 seconds for **BST** and **BAT** with 5% soil damping

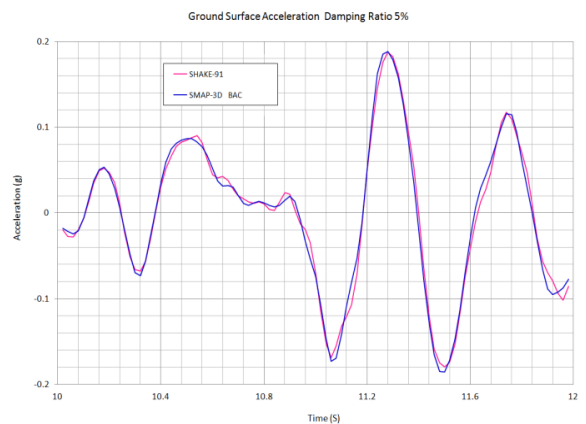


Fig. 8 Accelerations from 10 to 12 seconds for **BAC** with 5% soil damping

damping which represents an approximately average damping ratio at about 0.01% of shear strain level (Seed *et al.* 1970, Seed *et al.* 1986). Note that dampings below shear strain level of 0.001% in sand and silty sand are generally under 2% (Payan *et al.* 2016b, Senetakis and Payan 2018).

Three finite element solutions with **BST**, **BAT**, and **BAC** are compared with the closed-form solution of SHAKE91 in the frequency domain.

Fig. 6 shows ground surface accelerations for the whole period. Fig. 7 shows ground surface accelerations between 10 and 12 seconds where solutions from **BST** and **BAT** are directly compared with closed form solution of SHAKE91. Fig. 8 shows ground surface accelerations between 10 and 12 seconds where conventional **BAC** solution is directly compared with SHAKE91.

The results of both **BST** and **BAT** solutions are identical and are very close to SHAKE91 results. And results of conventional **BAC** solution are very close to SHAKE91 results. That is, the last term in the **BAT** model contributes very little influence on this site response with 5% soil damping.

Fig. 9 shows spectral accelerations on the ground surface and Fig. 10 shows a close-up view of spectral accelerations between 0.1 and 1 seconds. Results of all three models of **BST**, **BAT**, and **BAC** predicted very well the closed-form solution of SHAKE91.

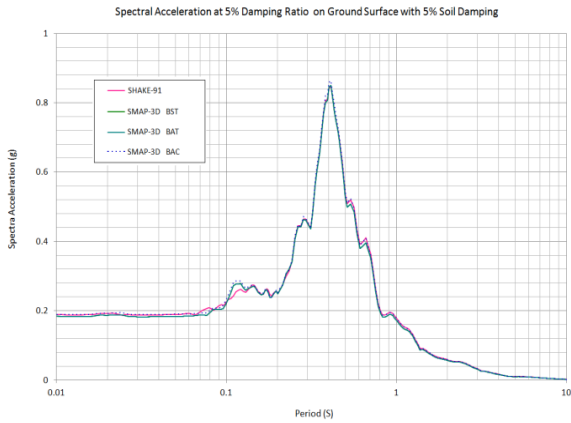


Fig. 9 Spectral accelerations on the ground surface with 5% soil damping

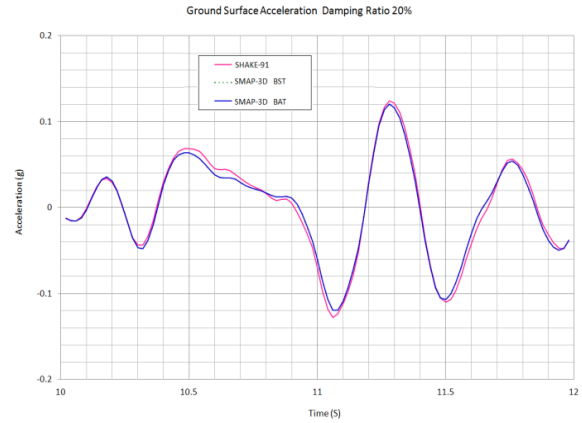


Fig. 12 Accelerations from 10 to 12 seconds for **BST** and **BAT** with 20% soil damping

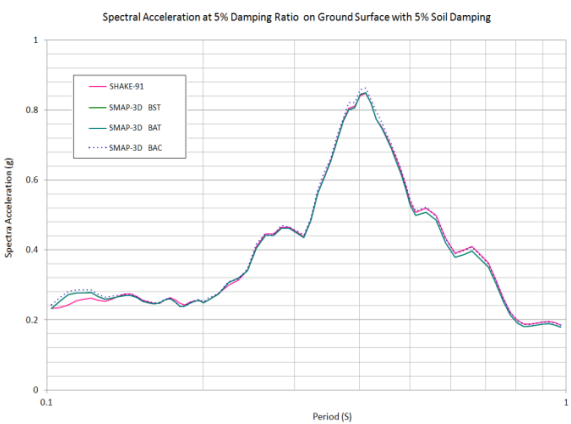


Fig. 10 Spectral accelerations from 0.1 to 1 second with 5% soil damping

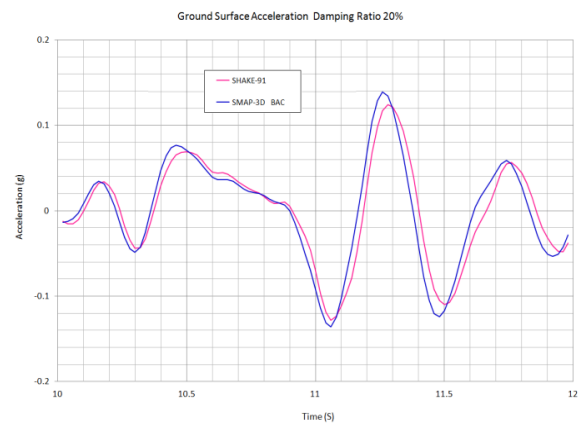


Fig. 13 Accelerations from 10 to 12 seconds for **BAC** with 20% soil damping

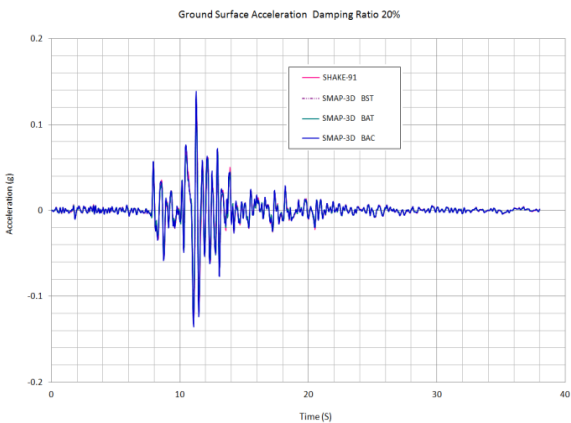


Fig. 11 Ground surface accelerations with 20% soil damping

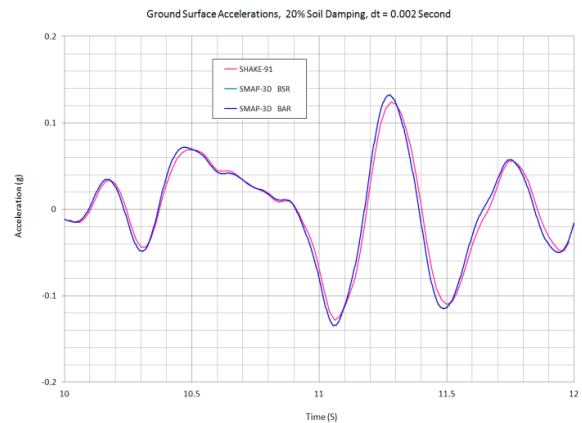


Fig. 14 Accelerations from 10 to 12 seconds for **BSR** and **BAR** with 20% soil damping

As the second set of analyses, we considered 20% soil damping which represents unrealistically high damping at extreme shear strain. Five finite element models with **BST**, **BAT**, **BAC**, **BSR**, and **BAR** are compared with the closed-form solution of SHAKE91 in the frequency domain.

Fig. 11 shows ground surface accelerations for the whole period for analyses of **BST**, **BAT**, and **BAC**. Fig. 12 shows ground surface accelerations between 10 and 12 seconds where solutions from **BST** and **BAT** are directly

compared with closed form solution of SHAKE91. Fig. 13 also shows ground surface accelerations between 10 and 12 seconds where conventional **BAC** solution is directly compared with SHAKE91. Fig. 14 shows the same close-up of accelerations of **BSR** and **BAR** solutions compared with SHAKE91.

The results of both **BST** and **BAT** solutions are identical and are very close to SHAKE91 results. However, the results of the conventional **BAC** solution show a shifting of

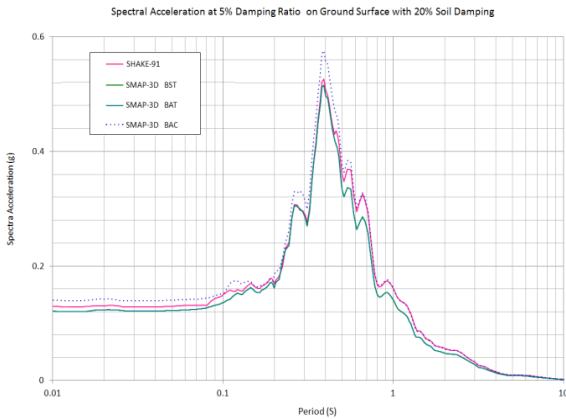


Fig. 15 Spectral accelerations on the ground surface with 20% soil damping

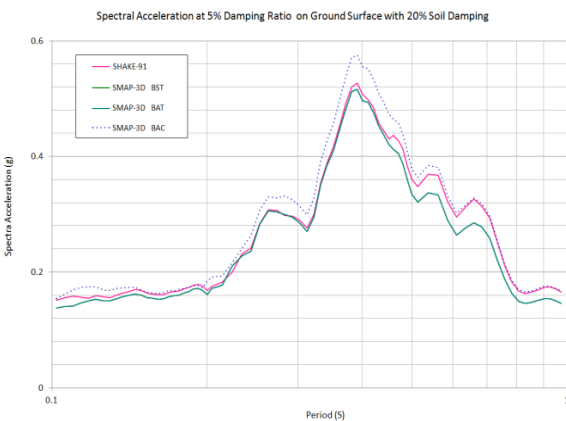


Fig. 16 Spectral accelerations from 0.1 to 1 second with 20% soil damping

the acceleration time history graph slightly to the left and show a somewhat higher acceleration response spectrum. The results of both **BSR** and **BAR** are almost identical and close to the SHAKE91 solution. Note that both **BSR** and **BAR** analyses used smaller time step-increment ($\Delta t=0.002$ sec) to get more accurate solutions.

Fig. 15 shows spectral accelerations on the ground surface and Fig. 16 shows a close-up view of spectral accelerations between 0.1 and 1 seconds. Compared with SHAKE91, both **BST** and **BAT** predicted very well while **BAC** predicted somewhat higher peak spectral acceleration.

7.2 Problem 2: Site response analysis to the Kobe earthquake

The second example problem is the site response analysis to the Kobe earthquake. The main purpose of this additional site response analysis is to verify that the base acceleration **BAT** model in terms of relative motions will produce the same results as the base shear **BST** model in terms of total motions. The second purpose is to assess the accuracy of the conventional finite element base acceleration **BAC** model where the equilibrium equation does not include the last term in the **BAT** model.

This problem is the same as the example problem enclosed in QUAD-4M User’s Manual (Hudson *et al.*

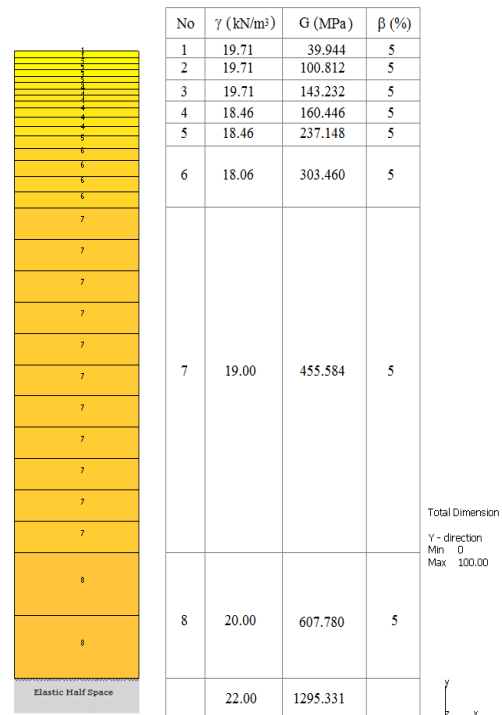


Fig. 17 Finite element meshes and material properties for Problem 2

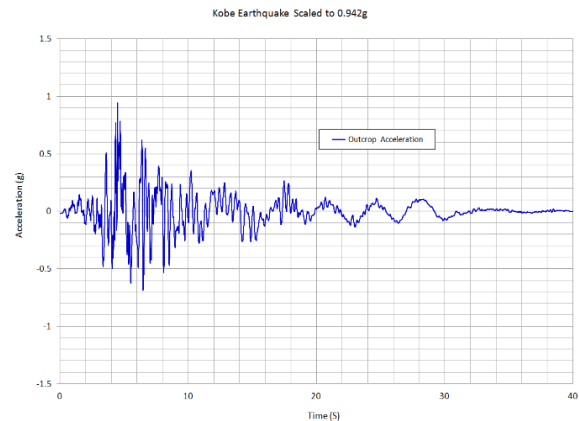


Fig. 18 Kobe earthquake acceleration time history

1994). A 100 m soil profile is subjected to the Kobe earthquake in 1995 as an outcrop to the elastic half-space. The earthquake is scaled to a peak acceleration of 0.942 g. Finite element meshes and material properties are shown in Fig. 17. The scaled earthquake time history and its spectral acceleration are shown in Figs. 18 and 19, respectively. The predominant period of the earthquake is about 0.25 seconds as shown in the response spectrum.

As the first set of analyses, we considered 5% soil damping used in Section 7.1. Three finite element solutions with **BST**, **BAT**, and **BAC** are compared with the closed-form solution of SHAKE91 in the frequency domain.

Fig. 20 shows ground surface accelerations for the whole period. Fig. 21 shows ground surface accelerations between 3 and 8 seconds where solutions from **BST** and **BAT** are directly compared with closed form solution of SHAKE91. Fig. 22 also shows ground surface accelerations

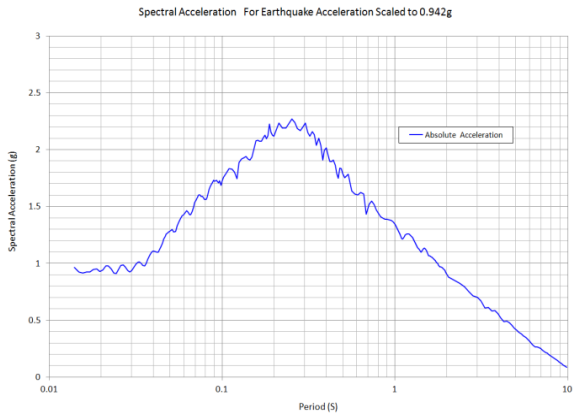


Fig. 19 Spectral acceleration for scaled Kobe earthquake

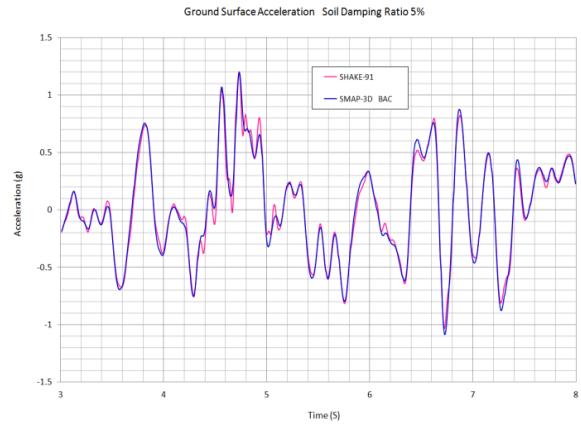


Fig. 22 Accelerations from 3 to 8 seconds for **BAC** with 5% soil damping

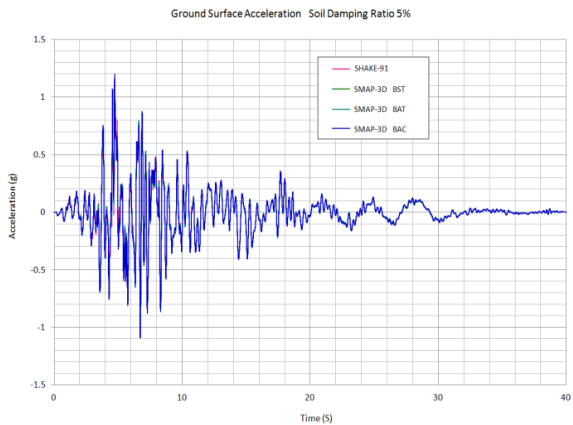


Fig. 20 Ground surface accelerations with 5% soil damping

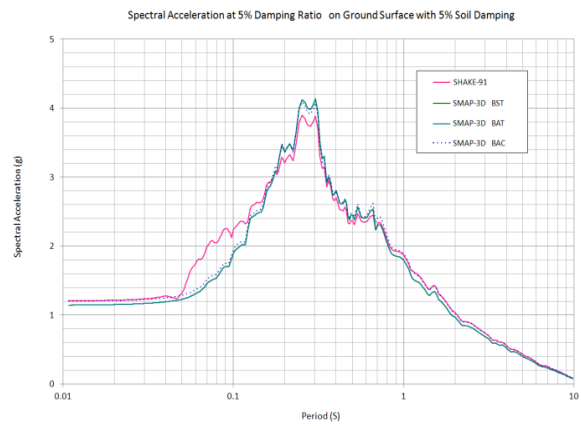


Fig. 23 Spectral accelerations on the ground surface with 5% soil damping

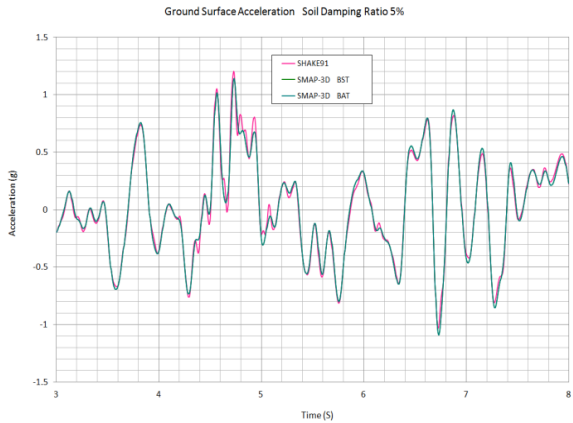


Fig. 21 Accelerations from 3 to 8 seconds for **BST** and **BAT** with 5% soil damping

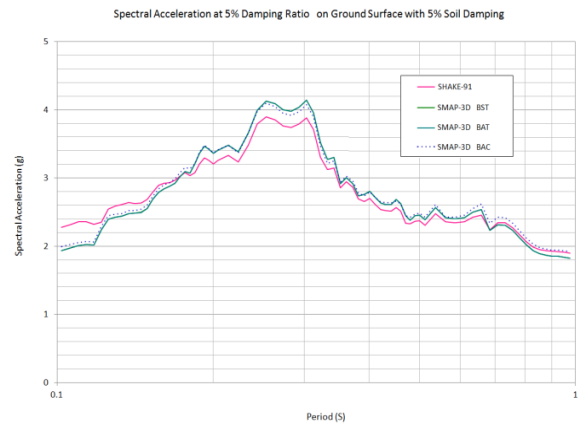


Fig. 24 Spectral accelerations from 0.1 to 1 second with 5% soil damping

between 3 and 8 seconds where conventional **BAC** solution is directly compared with SHAK91.

The results of both **BST** and **BAT** solutions are identical and are very close to SHAK91 results. And results of conventional **BAC** solution are close to SHAK91 results. That is, the last term in the **BAT** model contributes very little influence on this site response with 5% soil damping.

Fig. 23 shows spectral accelerations on the ground surface and Fig. 24 shows a close-up view of spectral accelerations between 0.1 and 1 seconds. Results of all three models of **BST**, **BAT**, and **BAC** show slightly higher

peak spectral accelerations than that of SHAK91.

As the second set of analyses, we considered 20% soil damping which represents unrealistically high damping at extreme shear strain. Five finite element solutions with **BST**, **BAT**, **BAC**, **BSR**, and **BAR** are compared with the closed-form solution of SHAK91 in the frequency domain.

Fig. 25 shows ground surface accelerations for the whole period for analyses of **BST**, **BAT**, and **BAC**. Fig. 26

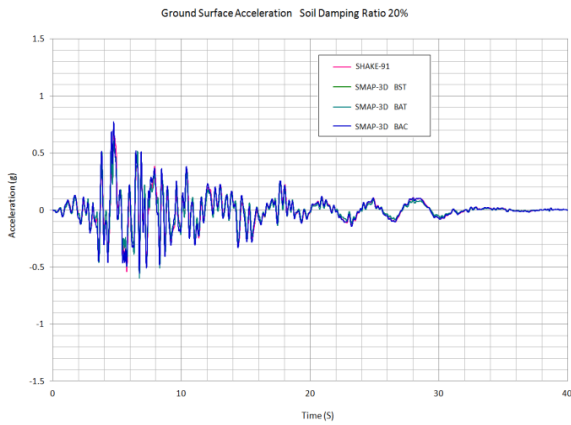


Fig. 25 Ground surface accelerations with 20% soil damping

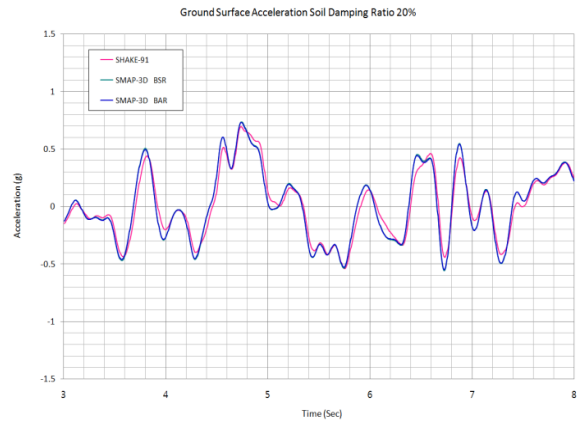


Fig. 28 Accelerations from 3 to 8 seconds for **BSR** and **BAR** with 20% soil damping

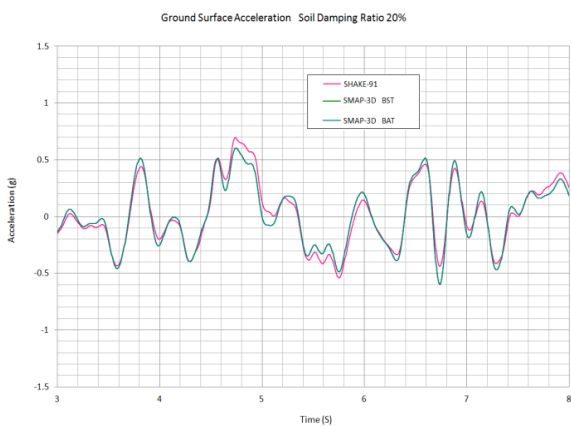


Fig. 26 Accelerations from 3 to 8 seconds for **BST** and **BAT** with 20% soil damping

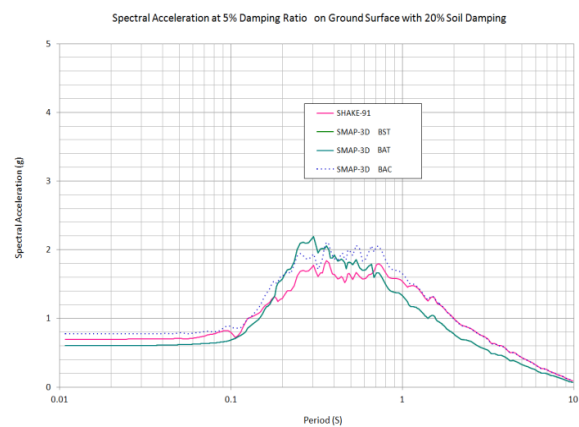


Fig. 29 Spectral accelerations on the ground surface with 20% soil damping

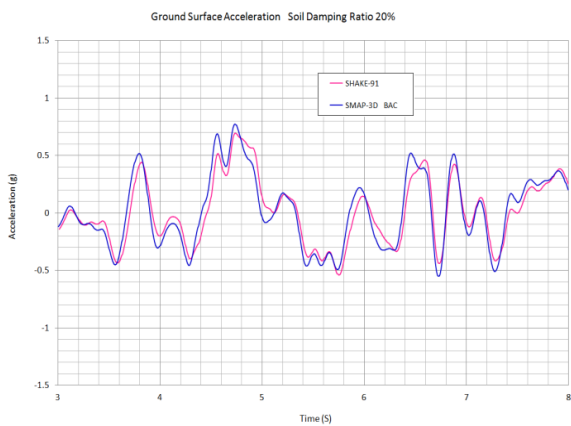


Fig. 27 Accelerations from 3 to 8 seconds for **BAC** with 20% soil damping

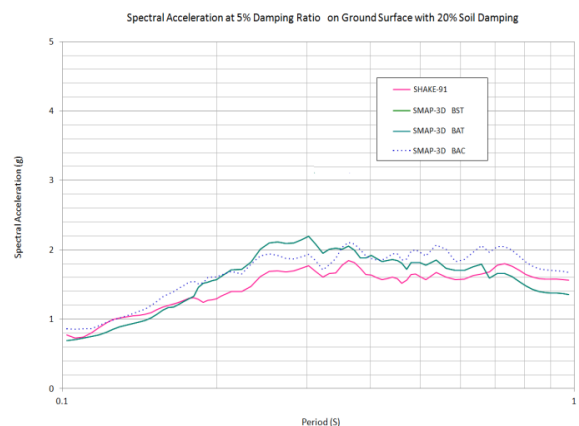


Fig. 30 Spectral accelerations from 0.1 to 1 second with 20% soil damping

shows ground surface accelerations between 3 and 8 seconds where solutions from **BST** and **BAT** are directly compared with closed form solution of SHAKE91. Fig. 27 shows ground surface accelerations between 3 and 8 seconds where conventional **BAC** solution is directly compared with SHAKE91. Fig. 28 shows the same close-up of accelerations of **BSR** and **BAR** solutions compared with SHAKE91.

The results of both **BST** and **BAT** solutions are identical

and are close to SHAKE91 results. However, the results of the conventional **BAC** solution show a shifting of the acceleration time history graph slightly to the left as in the case of the Diamond Heights earthquake with 20% soil damping in Example Problem I. The results of both **BSR** and **BAR** are almost identical and close to the SHAKE91 solution. It seems that the conventional base acceleration **BAC** procedure predicts reasonably well the site response in the soil profile with such high soil damping.

Table 1 Summary of dynamic equilibrium equations for earthquake load

Model	Dynamic Equilibrium Equation
BST	$\mathbf{M}\ddot{\mathbf{u}} + \mathbf{D}\dot{\mathbf{u}} + \mathbf{K}\mathbf{u} + \mathbf{J} \cdot \mathbf{C} \cdot \dot{\mathbf{u}}_{n+1} = \mathbf{J} \cdot \mathbf{F}_s$
BAT	$\mathbf{M}\ddot{\mathbf{u}}_r + \mathbf{D}\dot{\mathbf{u}}_r + \mathbf{K}\mathbf{u}_r + \mathbf{J} \cdot \mathbf{C} \cdot \dot{\mathbf{u}}_{rn+1} = -\mathbf{M} \cdot \mathbf{I} \cdot \ddot{\mathbf{u}}_g - \mathbf{a} \cdot \mathbf{M} \cdot \mathbf{I} \cdot \dot{\mathbf{u}}_g$
BAC	$\mathbf{M}\ddot{\mathbf{u}}_r + \mathbf{D}\dot{\mathbf{u}}_r + \mathbf{K}\mathbf{u}_r + \mathbf{J} \cdot \mathbf{C} \cdot \dot{\mathbf{u}}_{rn+1} = -\mathbf{M} \cdot \mathbf{I} \cdot \ddot{\mathbf{u}}_g$
BSR	$\mathbf{M}\ddot{\mathbf{u}} + \mathbf{D}\dot{\mathbf{u}} + \mathbf{K}\mathbf{u} + (\mathbf{C} \cdot \mathbf{J} - \mathbf{a} \cdot \mathbf{M} \cdot \mathbf{I}) \cdot \dot{\mathbf{u}}_{n+1} = \mathbf{J} \cdot \mathbf{F}_s$
BAR	$\mathbf{M}\ddot{\mathbf{u}}_r + \mathbf{D}\dot{\mathbf{u}}_r + \mathbf{K}\mathbf{u}_r + (\mathbf{C} \cdot \mathbf{J} - \mathbf{a} \cdot \mathbf{M} \cdot \mathbf{I}) \cdot \dot{\mathbf{u}}_{rn+1} = -\mathbf{M} \cdot \mathbf{I} \cdot \ddot{\mathbf{u}}_g$

Fig. 29 shows spectral accelerations on the ground surface and Fig. 30 shows a close-up view of spectral accelerations between 0.1 and 1 seconds. Compared with SHAKE91, the results of all three models of **BST**, **BAT**, and **BAC** predicted somewhat higher peak spectral accelerations.

8. Conclusions

Dynamic equilibrium equations, as summarized in Table 1, were derived for the free field one-dimensional shear wave propagation through the horizontally layered soil deposits with the elastic half-space. We expressed Rayleigh's viscous damping consisting of mass and stiffness proportional terms.

We considered two cases where damping matrices are defined in the total and relative displacement fields. Two forms of equilibrium equations are presented; one in terms of total motions and the other in terms of relative motions.

When the damping matrix is defined in the total displacement field, both **BST** in total motions and **BAT** in relative motions are obtained. It was noted that the conventional finite element procedure **BAC** is missing the term $-\mathbf{a} \cdot \mathbf{M} \cdot \mathbf{I} \cdot \dot{\mathbf{u}}_g$ as included in the **BAT** model.

When the damping matrix is defined in the relative displacement field, both **BSR** in total motions and **BAR** in relative motions are obtained. Both **BSR** and **BAR** contain a term with the product of $(\mathbf{a} \cdot \mathbf{M} \cdot \mathbf{I})$ and the interface velocity $(\dot{\mathbf{u}}_{n+1}, \dot{\mathbf{u}}_{n+1})$. The inclusion of such a term can lead to a non-symmetric full matrix for the solution. To take advantage of the banded symmetric matrix form, we can move this term to the right-hand side of the equal sign and then perform iterations or use smaller time increments.

Two example problems were presented. The main purpose of these site response analyses is to verify that the base acceleration **BAT** model in terms of relative motions will produce the same results as the base shear **BST** model in terms of total motions. The second purpose is to assess the accuracy of the conventional finite element base acceleration **BAC** model where the equilibrium equation does not include the last term in the **BAT** model.

Based on our study, the **BST** model is the simpler form of equilibrium equation to be used for finite element formulation and the conventional finite element procedure **BAC** model predicts the exact solution reasonably well even in soil deposits with unrealistically high damping.

Acknowledgments

This work was partially supported by the "Radioactive Waste Management Program" of the Korea Institute of Energy Technology Evaluation and Planning (KETEP) granted financial resources from the Ministry of Trade, Industry and Energy, Republic of Korea (Project No. 20193210100040).

References

- Ameri, G., Baumont, D., Shible, H., Ego, F. and Contrucci, I. (2023), "Characterizing site-specific ground motion at great depth in a low seismicity region: Challenges and perspectives for a nuclear waste repository project", *Bull. Earthq. Eng.*, **21**, 4755-4787. <https://doi.org/10.1007/s10518-023-01720-z>.
- Astroza, R., Pasten, C. and Ochoa-Cornejo, F. (2017), "Site response analysis using one-dimensional equivalent-linear method and Bayesian filtering", *Comput. Geotech.*, **89**, 43-54. <https://doi.org/10.1016/j.compgeo.2017.04.004>.
- Chatterjee, K., Choudhury, D. and Poulos, H.G. (2015), "Seismic analysis of laterally pile under influence of vertical loading using finite element method", *Comput. Geotech.*, **67**, 172-186. <https://doi.org/10.1016/j.compgeo.2015.03.004>.
- Comtec Research (2022), SMAP-3D; Structure Medium Analysis Program, User's Manual Version 7.05, Comtec Research, Seoul, Korea.
- Desai, C.S. and Christian J.T. (1977), *Numerical Methods in Geotechnical Engineering. Chapter 19: Soil Amplification of Earthquakes and Chapter 20: Two- and Three-Dimensional Dynamic Analyses*, McGraw Hill Company, New York, NY, USA.
- Dikmen, S.U. and Ghaboussi, J. (1984), "Effective stress analysis of seismic response and liquefaction: Theory", *J. Geotech. Eng. ASCE*, **110**(5), 628-644. [https://doi.org/10.1061/\(ASCE\)0733-9410\(1984\)110:5\(628\)](https://doi.org/10.1061/(ASCE)0733-9410(1984)110:5(628)).
- Germoso C., Duval J.L. and Chinesta, F. (2020), "Harmonic-modal hybrid reduced order model for the efficient integration of non-linear soil dynamics", *Appl. Sci.*, **10**(19), 6778. <https://doi.org/10.3390/app10196778>.
- Ghaemmaghami, A.R., Mercan, O. and Kianoush, R. (2017), "Seismic soil-structure analysis of wind turbines in frequency domain", *Wind Energy*, **20**, 125-142. <https://doi.org/10.1002/we.1995>.
- Hardin, B.O. and Drnevich, V.P. (1972a), "Shear modulus and damping in soils: measurement and parameter effects (Terzaghi lecture)", *J. Soil Mech. Found. Div. ASCE*, **98**(6), 603-624. <https://doi.org/10.1061/JSFEAQ.0001756>.
- Hardin, B.O. and Drnevich, V.P. (1972b), "Shear modulus and damping in soils: design equations and curves", *J. Soil Mech. Found. Div. ASCE*, **98**(7), 667-692. <https://doi.org/10.1061/JSFEAQ.0001760>.
- Hudson, M. (1994), "Behavior of slopes and earth dams during earthquakes", Doctoral Thesis, University of California, Davis, California, USA.
- Hudson, M., Idriss, I.M. and Beikae, M. (1994), "User's manual for QUAD4M: A computer program to evaluate the seismic response of soil structures using finite element procedures and incorporating a compliant base", University of California, Davis, CA, USA.
- Idriss, I.M. and Sun, J.I. (1992), "User's manual for SHAKE91: A computer program for conducting equivalent linear seismic response analyses of horizontally layered soil deposits", Center for Geotechnical Modeling, Department of Civil & Environmental Engineering, University of California, Davis,

- CA, USA.
- Joyner, W.B. and Chen, A.T.F. (1975), "Calculation of nonlinear ground response in earthquakes", *Bull. Seismol. Soc. Am.*, **565**(5), 1315-1336. <https://doi.org/10.1785/BSSA0650051315>.
- Lai, C.G. and Rix, G.J. (1988), "Simultaneous inversion of Rayleigh phase velocity and attenuation for near-surface site characterization", Report No. GIT-CEE/GEO-98-2; School of Civil and Environmental Engineering, Georgia Institute of Technology, Atlanta, GA, USA.
- Liu, G., Lian, J. and Zhao, M. (2017), "An effective approach for simulating multi-support earthquake underground motions", *Bull. Earthq. Eng.*, **15**, 4635-4659. <https://doi.org/10.1007/s10518-017-0153-3>.
- Newmark, N.M. (1959), "A method of computation for structural dynamics", *J. Eng. Mech. Div. ASCE*, **85**(3), 67-94. <https://doi.org/10.1061/JMCEA3.0000098>.
- Ordonez, G.A. (2012), "SHAKE2000: A computer program for the 1-D analysis of geotechnical earthquake engineering problems", Geomotions, LLC, Lacey, WA, USA.
- Payan, M. (2017), "Study of small strain dynamic properties of sands and silty sands", Doctoral Dissertation, The University of New South Wales, Sydney, Australia.
- Payan, M., Khoshghalb, A., Senetakis, K. and Khalili, N. (2016a), "Small-strain stiffness of sand subjected to stress anisotropy", *Soil Dyn. Earthq. Eng.*, **88**, 143-151. <https://doi.org/10.1016/j.soildyn.2016.06.004>.
- Payan, M., Senetakis, K., Khoshghalb, A. and Khalili, N. (2016b), "Influence of particle shape on small-strain damping ratio of dry sands", *Geotech.*, **66**(7), 610-616. <https://doi.org/10.1680/jgeot.15.T.035>.
- Rayleigh, J. and Lindsay, R. (1945), *The Theory of Sound*, Dover Publications Inc., Garden City, NY, USA.
- Schnabel, P.B., Lysmer, J. and Seed, H.B. (1972), "SHAKE: A computer program for earthquake response analysis of horizontally layered sites", Report No. UCB/EERC-72/12; Earthquake Engineering Research Center, University of California, Berkeley, CA, USA.
- Seed, H.B. and Idriss, I.M. (1970), "Soil moduli and damping factors for dynamic response analysis", Report No. EERC 75-29; Earthquake Engineering Research Center, University of California, Berkeley, CA, USA.
- Seed, H.B., Wong, R.T., Idriss, I.M. and Tokimatsu, K. (1986), "Moduli and damping factors for dynamic analyses of cohesive soils", *J. Geotech. Eng. ASCE*, **112**(11), 1016-1032. [https://doi.org/10.1061/\(ASCE\)0733-9410\(1986\)112:11\(1016\)](https://doi.org/10.1061/(ASCE)0733-9410(1986)112:11(1016)).
- Senetakis, K. and Payan, M. (2018), "Small strain damping ratio of sands and silty sands subjected to flexural and torsional resonant column excitation", *Soil Dyn. Earthq. Eng.*, **114**, 448-459. <https://doi.org/10.1016/j.soildyn.2018.06.010>.
- Tran, N.L., Aaqib, M., Nguyen, B.P., Nguyen, D.D., Tran, V.L. and Nguyen, V.Q. (2021), "Evaluation of seismic site amplification using 1D site response analyses at Ba Dinh Square Area, Vietnam", *Adv. Civil Eng.*, **2021**, 3919281. <https://doi.org/10.1155/2021/3919281>.
- Tsai, N.C. (1969), "Influence of local geology on earthquake ground motions", Ph.D. Thesis, California Institute of Technology, Pasadena, CA, USA.
- Volpini, C., Douglas, J. and Nielsen, A.H. (2021), "Guidance on conducting 2D linear viscoelastic site response analysis using a finite element code", *J. Earthq. Eng.*, **25**(6), 1153-1170. <https://doi.org/10.1080/13632469.2019.1568931>.
- Watanabe, K., Pisano, F. and Jeremic, B. (2017), "Discretization effects in the finite element simulation of seismic waves in elastic and elastic-plastic media", *Eng. Comput.*, **33**, 519-545. <https://doi.org/10.1007/s00366-016-0488-4>.
- Xu, C., Liu, Q., Tang, X., Sun, L., Deng, P. and Liu, H. (2023), "Dynamic stability analysis of jointed rock slopes using the combined finite discrete element method (FDEM)", *Comput. Geotech.*, **160**, 105556. <https://doi.org/10.1016/j.compgeo.2023.105556>.

CC

Notations

u_g	Input earthquake outcrop displacement on the surface of elastic half-space
\dot{u}_g	Input earthquake outcrop velocity on the surface of elastic half-space
\ddot{u}_g	Input earthquake outcrop acceleration on the surface of elastic half-space
u_{n+1}	Total displacement on the surface of elastic half-space
\dot{u}_{n+1}	Total velocity on the surface of elastic half-space
\ddot{u}_{n+1}	Total acceleration on the surface of elastic half-space
u_{rn+1}	Relative displacement on the surface of elastic half-space, $u_{rn+1} = u_{n+1} - u_g$
\dot{u}_{rn+1}	Relative velocity on the surface of elastic half-space, $\dot{u}_{rn+1} = \dot{u}_{n+1} - \dot{u}_g$
\ddot{u}_{rn+1}	Relative acceleration on the surface of elastic half-space, $\ddot{u}_{rn+1} = \ddot{u}_{n+1} - \ddot{u}_g$
u	Total displacement vector
\dot{u}	Total velocity vector
\ddot{u}	Total acceleration vector
I	Unit vector at all rows, $I^T = \langle 1, 1, \dots, 1, 1 \rangle$
J	Unit vector at last row, $J^T = \langle 0, 0, \dots, 0, 1 \rangle$
0	Zero vector at all rows, $0^T = \langle 0, 0, \dots, 0, 0 \rangle$
u_r	Relative displacement vector, $u_r = u - I \cdot u_g$
\dot{u}_r	Relative velocity vector, $\dot{u}_r = \dot{u} - I \cdot \dot{u}_g$
\ddot{u}_r	Relative acceleration vector, $\ddot{u}_r = \ddot{u} - I \cdot \ddot{u}_g$
M	Mass matrix
D	Damping matrix
K	Stiffness matrix
ρ_r	Rock mass density of elastic half-space
c_{sr}	Rock shear wave velocity of elastic half-space
A_s	a Tributary area on the surface of elastic half-space
C	Damping constant, $C = \rho_r \cdot c_{sr} \cdot A_s$
F_s	Base shear force, $F_s = C \cdot \dot{u}_g$
a	Rayleigh mass proportional damping constant
b	Rayleigh stiffness proportional damping constant
β	Critical damping ratio in an element
ω_1	Fundamental natural circular frequency of the system
ω_I	Predominant circular frequency of the input earthquake motion
Δt	Time step increment for a step-by-step solution